Available online at www.sciencedirect.com
ScienceDirect
Geomorphology 99 (2008) 139–149
GEOMORPHOLOGY
www.elsevier.com/locate/geomorph

# Unraveling complex exposure-burial histories of bedrock surfaces under ice sheets by integrating cosmogenic nuclide concentrations with climate proxy records

Yingkui Li [a,*], Derek Fabel [b], Arjen P. Stroeven [c], Jon Harbor [d]

[a] Department of Geography, University of Missouri–Columbia, Columbia, MO 65211, USA
[b] Department of Geographical and Earth Sciences, University of Glasgow, Glasgow, G12 8QQ, UK
[c] Department of Physical Geography and Quaternary Geology, Stockholm University, S-106 91 Stockholm, Sweden
[d] Department of Earth and Atmospheric Sciences, Purdue University, West Lafayette, IN 47906, USA

Received 19 June 2007; received in revised form 15 October 2007; accepted 17 October 2007
Available online 3 December 2007

**Abstract**

The production, accumulation, and decay of cosmogenic radionuclides in rock surfaces subjected to episodes of exposure and burial by ice results in nuclide concentrations in present day rock surfaces that can be used to address a variety of questions in glacial geomorphology and Quaternary geology. Of particular importance is the fact that these nuclide concentrations reflect both the timing of initial exposure of the rock surface and the chronology of subsequent exposure, burial, and erosion episodes. For landscapes where geomorphic evidence indicates that little/no erosion occurred, constraining the timing of initial exposure and the number of phases of exposure and burial that a rock surface has been subjected to is possible using multiple cosmogenic radionuclide concentrations combined with proxies for the timing and duration of periods of ice cover, such as ice core or marine isotope records. However, interpretations based on this approach require determination of an appropriate cutoff value to separate the proxy record into ice-free and ice-covered conditions and assessment of the sensitivity of the results to different cutoff values.

We have developed a numerical model to evaluate variations in total exposure and burial durations as a function of different proxy records and cutoff values. This program is available at http://www.missouri.edu/~liyk/ClimateProxyCurve.zip. Initial results for sites in West Antarctica and northern Sweden show that the method provides a quick and robust way to derive best-fit cutoff values and chronologies of burial and exposure, and small changes in cutoff values can result in significant shifts in results. The method described here provides new insight into the interpretation and reliability of multiple nuclide samples. This approach also has the potential to provide improved constraints for ice sheet dynamics and landscape evolution, and a means to assess the sensitivity of calculated initial exposure dates to assumptions about ice sheet history.


*Keywords:* Cosmogenic nuclides; Ice sheet; Complex burial-exposure histories; Surface exposure dating

## 1. Introduction

Interpretations of concentrations of cosmogenic nuclides in rocks from surfaces formerly covered by ice sheets are now routinely used in reconstructing the dynamics of ice sheets and in examining landscape evolution under ice sheets (e.g., Fabel et al., 2002; Stroeven et al., 2002a,b; Stone et al., 2003; Li et al., 2005; Staiger et al., 2005; Sugden et al., 2005; Harbor et al., 2006). Cosmogenic nuclide surface exposure dating of glacial landforms that indicate the positions of former ice margins has been used to constrain chronologies of ice sheet advances and retreats for the Antarctic (Brook et al., 1993), Laurentide (Steig et al., 1998; Bierman et al., 1999; Davis et al., 1999; Marsella et al., 2000; Balco et al., 2002), and Fennoscandian ice sheets (Tschudi et al., 2000; Rinterknecht et al., 2004, 2005, 2006, 2007). Measurements of nuclide concentrations for bedrock surfaces and erratics within the extent of former ice sheets have also been used to discriminate basal thermal conditions and erosion patterns under ice sheets. For example, this approach has been used to examine the history of supposed nunataks (Brook et al., 1996; Stone et al., 1998; Landvik et al., 2003;

* Corresponding author. Tel.: +1 573 882 2879; fax: +1 573 884 4239.
*E-mail address:* liyk@missouri.edu (Y. Li).

0169-555X/$ - see front matter © 2007 Elsevier B.V. All rights reserved.
doi:10.1016/j.geomorph.2007.10.010

Nesje et al., 2007) and to constrain erosion volumes and rates in stoss and lee topography (Briner and Swanson, 1998) and valley systems (Fabel et al., 2004; Li et al., 2005; Staiger et al., 2005; Sugden et al., 2005). These studies have provided much needed confirmation of ice sheet dynamics and significant new insights into landscape evolution under ice sheets.

Of particular interest in studies of some former ice sheets has been the presence of relict bedrock surfaces that have been preserved with little or no alteration despite being covered by ice sheets (e.g., Fabel et al., 2002; Stroeven et al., 2002b, 2006; Briner et al., 2003; Marquette et al., 2004; Sugden et al., 2005; Harbor et al., 2006; Phillips et al., 2006). These surfaces provide intriguing possibilities to identify basal conditions under former ice sheets (Goodfellow, 2007), which can be of particular importance in constraining basal thermal boundary conditions for numerical ice sheet models (Staiger et al., 2005). Recently, measurements of cosmogenic nuclides in relict bedrock surfaces were also used to interpret how many glacial cycles a relict surface has survived without significant erosion (Fabel et al., 2002; Stroeven et al., 2002b; Sugden et al., 2005). This is achieved by modeling the accumulation and decay of cosmogenic nuclides through a reconstructed history of exposure and burial based on climate proxy records, using assumptions of appropriate cutoff values to determine ice cover or exposure for particular locations (Fig. 1). This approach, typically comparing ratios of nuclides such as $^{26}Al/^{10}Be$ in bedrock quartz with proxy records such as benthic foraminifera oxygen isotope curves from marine sediments, has considerable potential to expand our understanding of complex exposure-burial histories for relict bedrock surfaces under ice sheets (Fabel et al., 2002; Stroeven et al., 2002b; Sugden et al., 2005; Phillips et al., 2006) and of ice sheet behavior over sequences of glaciations. The ability to better constrain ice sheet behavior over sequences of glaciations is of particular importance for ice sheet modeling (Napieralski et al., 2007) and for integrated studies of crustal responses to changing glacial and marine limits (e.g., van den Berg, 2007).

A key element of this approach to reconstructing burial and exposure history is the specification of a cutoff value that is used to determine ice-free and ice-covered periods from a specific climate proxy record. In initial developments of this approach, considerable effort was put into examining records of Quaternary climate change and corresponding ice sheet marginal records as a basis for proposing cutoff values for mountain glaciation and ice sheet glaciation in northern Sweden (Kleman and Stroeven, 1997; Stroeven et al., 2002b). After manually examining several possible cutoff values in terms of the predicted record compared to the existing records for the timing and duration of ice-free and ice-covered periods during the last glacial cycle in northern Sweden, the authors proposed an initial best-fit cutoff value of 3.7‰ using a DSDP 607 record (Fig. 1).

An element of subjectivity and a large amount of laborious work exist in this approach to arrive at cutoff values, which are also likely to vary with locations for studies on the scale of a large ice sheet. We have therefore developed a numerical approach that uses nuclide concentrations and multiple nuclide ratios in an iterative process to determine a best-fit cutoff value for a particular location and climate proxy record. This approach also allows a user to examine the sensitivity of evaluations of complex exposure history to the selection of the cutoff value and to evaluate the impact of uncertainties in the measurements of cosmogenic nuclide concentrations on derived complex exposure histories. This paper introduces the method for evaluating complex exposure-burial histories of relict bedrock surfaces by integrating climatic proxy records with cosmogenic nuclide pairs ($^{10}Be$ and $^{26}Al$) and tests its applicability using published data from West Antarctica and northern Sweden.

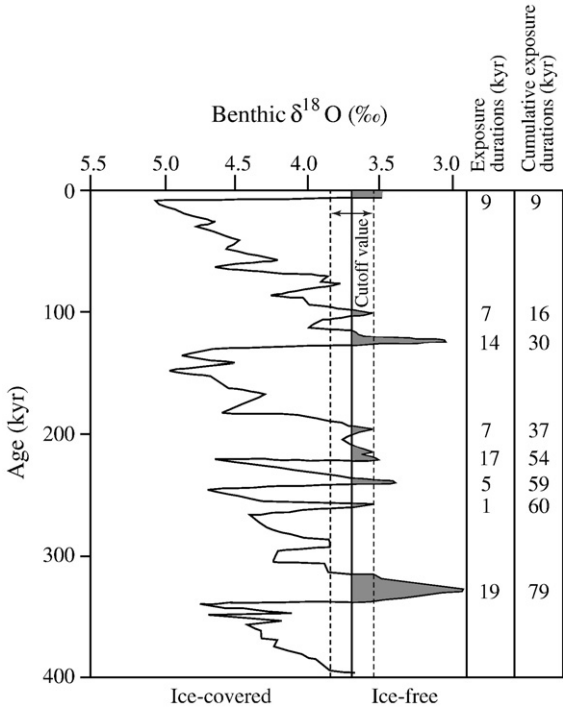


Fig. 1. Marine benthic foraminifera oxygen isotope record for the last 400 kyr from DSDP 607 (Lazarus et al., 1995) modified from Fabel et al. (2002) and Stroeven et al. (2002b). Ice-covered and ice-free periods for study sites in northern Sweden were based on the cutoff value of $\delta^{18}O=3.7‰$ proposed by Kleman and Stroeven (1997). Surface exposure occurs during ice-free periods and results in exposure durations shown in the gray shaded areas on the right side of the cutoff line and as a cumulative total. Time periods on the left side of the cutoff line represent periods of surface burial by ice. Shifting the cutoff value (indicated by double-headed arrow and dashed line) results in changes in exposure- and burial durations. Cosmogenic radionuclides, such as $^{10}Be$ and $^{26}Al$, accumulate in the rock surfaces during periods of exposure, and continue to decay during periods of ice cover at rates that depend on the half life of each radionuclide. Using the exposure and burial history determined by the cutoff value, $^{10}Be$ and $^{26}Al$ concentrations and $^{26}Al/^{10}Be$ ratios can be simulated to determine the best-fit cutoff value and total exposure-burial history of a sample surface.

## 2. Methodology

Changes in global and regional ice volumes are indirectly recorded in proxy records obtained from sources such as marine sediments, coral reefs, and ice cores (e.g., Shackleton and

Opdyke, 1973; Shackleton, 1984; Lazarus et al., 1995; Mangerud et al., 1996; Turco et al., 2001; Vidal et al., 2002; Spielhagen et al., 2004; Westerhold et al., 2005). These proxy records for ice volume can, perhaps, be used to study the volumetric behavior of a specific ice sheet if the ice sheets behaved in concert with the proxies. Modeling studies by Bintanja et al. (2002, 2005) showed that while this is not true in detail, because the record is simply dominated by the behavior of the largest ephemeral ice sheet (i.e., the Laurentide Ice Sheet), however as a first approximation this reasoning can be applied to the Antarctic and Fennoscandian ice sheets under investigation here. Given the assumption that temporal variations in a proxy record provide an indication of temporal variations in ice sheet volume and extent, a cutoff value can be adopted that divides the proxy record into ice-free and ice-covered periods for a particular location of interest (Fig. 1). In this study, a suite of modeled accumulation and decay histories of cosmogenic nuclides based on different cutoff values is compared to measured nuclide concentrations to determine the best-fit cutoff value and initial exposure time for particular sites of interest.

This methodology has been implemented through an iterative process using $^{10}$Be and $^{26}$Al. Fig. 2 provides a flowchart and interface of the program we developed. The program input parameters include measured $^{10}$Be and $^{26}$Al concentrations (atoms g$^{-1}$), their uncertainties (atoms g$^{-1}$) and production rates (atoms g$^{-1}$ yr$^{-1}$), rock density (g cm$^{-3}$), cosmic ray mean free path (g cm$^{-2}$), subaerial erosion rate (cm kyr$^{-1}$), glacial erosion rate (cm kyr$^{-1}$), and the choice of climate proxy record. The results are recorded in an output text file and a summary is presented in the list box of the program interface.

Based on the range of values of the specified climate proxy record, the first routine assembles a suite of cutoff values varying from its minimum value ($V_{min}$) to its maximum value ($V_{max}$):

$$\text{Cutoff}_i = V_{\min} + i^{*}V_{\text{int}} \quad (1)$$

where Cutoff$_i$ is the cutoff value for the $i$-th iteration and $i$ is the number of intervals used to adjust the cutoff value. In order to examine in detail the sensitivity of the results to cutoff values, the interval used here, $V_{int}$, is defined as 1/1000 of the range of the proxy climate record ($V_{max} - V_{min}$). Thus, the first routine yields 1000 cutoff values ranging from the minimum value to the maximum value of the climate proxy record.

For each cutoff value, further routines divide the climate proxy record into ice-free and ice-covered periods (cf. Fig. 1) and simulate "time integrated" $^{10}$Be concentrations from assumed initial exposures during different ice-free periods. Because a $^{10}$Be apparent exposure age calculated using the zero erosion assumption is the minimum exposure time of a surface (Lal, 1991; Gosse and Phillips, 2001), the program uses this as a time constraint and only simulates complex histories where the cumulative exposure is larger than the $^{10}$Be apparent exposure age. Hence, for some cutoff values close to $V_{min}$ (cf. Fig. 1), the total exposure duration for all ice-free periods within the time range of the climate proxy record is less than the $^{10}$Be apparent exposure age and these cutoff values are disregarded entirely. During the simulations, the program will store when the simulated "time integrated" $^{10}$Be concentration reaches <0.1% difference of the measured $^{10}$Be concentration. Such simulations define a best-fit for this cutoff value and the program will then simulate the corresponding $^{26}$Al concentration using the

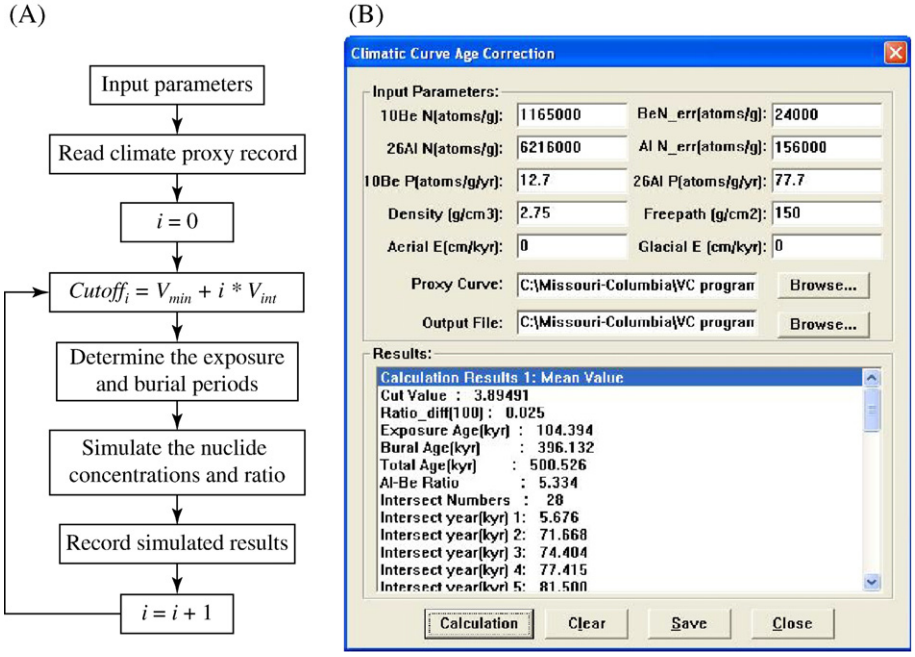


Fig. 2. Flow chart showing the iterative process used to determine the appropriate cutoff value and assess the sensitivity of the results to different cutoff values (A) and a program interface to show the required input parameters and the results (B). This program is available at http://www.missouri.edu/~liyk/ClimateProxyCurve.zip.

same history and calculate the $^{26}Al/^{10}Be$ ratio. All results for this cutoff value are recorded and the difference between simulated and measured $^{26}Al/^{10}Be$ ratios is used as an index to compare with other simulations using different cutoff values.

Using an iterative process, the differences between simulated and measured $^{26}Al/^{10}Be$ ratios are compared for all examined cutoff values. The cutoff value with the minimum ratio difference is considered to be the best-fit cutoff value. The simulation processes and the best-fit results are recorded and summarized into an output file and the list box of the program interface. The parameters summarized in the list box include the best-fit cutoff value, $^{26}Al/^{10}Be$ ratio difference, total exposure duration, total burial duration, total complex history, and the numbers of intersections between the best-fit cutoff value and the climate proxy record and the corresponding time for each intersection.

Another routine provides an assessment of the uncertainties of the results based on the measured uncertainties of the $^{10}Be$ and $^{26}Al$ concentrations. This is accomplished by examining all possible combinations of $^{10}Be$ and $^{26}Al$ concentrations adjusted by their measured uncertainties, searching the best solution for each combination, and summarizing the range of values for each output parameter of interest. An additional routine can examine potential erosion rates during ice-free and ice-covered periods. When subaerial and glacial erosion rates are varied on the program interface, the user can test the sensitivity of results to erosion rates and evaluate the maximum allowable erosion rates for ice-free and ice-covered periods.

The methodology is only applicable for samples where the measured $^{26}Al/^{10}Be$ ratio reflects a complex exposure-burial history (i.e. when the ratio is lower than the production ratio of these two nuclides (around 6.1) with a statistically significant difference). Burial of a surface by several tens of meters of ice results in complete shielding of the surface from cosmic rays. Cosmogenic nuclides accumulated prior to the burial period will continue to decay, with $^{26}Al$ decaying about twice as fast as $^{10}Be$, causing the $^{26}Al/^{10}Be$ ratio to decrease exponentially (Lal, 1991; Fabel and Harbor, 1999). In cases we have examined, based on measured concentrations of multiple cosmogenic nuclides ($^{10}Be$ and $^{26}Al$) and their *in situ* production rates, the proposed method can be used to determine an appropriate best-fit cutoff value for the climate proxy record, assess the sensitivity of results to different cutoff values, and evaluate complex exposure-burial histories of the investigated surfaces. In the next section, we illustrate the approach using datasets from West Antarctica and northern Sweden.

## 3. Examples and applications of the approach

### 3.1. West Antarctica

In the coastal mountains of Marie Byrd Land, West Antarctica, ice-moulded bedrock surfaces occur below nunatak summits with weathered surfaces and tors (Sugden et al., 2005). Exposure of such rock surfaces implies that the thickness of the ice sheet has varied over time, leading to a spatially varied pattern of ice cover and exposure. Bedrock samples taken from several different locations (Sugden et al., 2005) show higher nuclide concentrations on the summits than on the ice-moulded slopes. This is consistent with an interpretation based on field investigations that the upstanding summit with weathered surfaces, tors, and granular granite grus was preserved during periods of ice sheet cover, whereas the ice-moulded slopes were subject to glacial erosion (Sugden et al., 2005).

Five samples (four from summit (relict) surfaces and one from the ice-moulded slopes) with measured $^{10}Be$ and $^{26}Al$ concentrations were analyzed (Table 1). The four summit samples show a range of old apparent exposure ages between 42.4±2.8 and 112.2±7.1 kyr (Table 2, inferred using measured $^{10}Be$ concentrations) and long apparent burial durations between $174.7^{+63.2}_{-61.1}$ and $263.0^{+58.7}_{-57.0}$ kyr (inferred from $^{26}Al/^{10}Be$ ratios). In contrast, the sample taken from the ice-moulded landforms has a young 4.5±0.5 kyr apparent exposure age ($^{10}Be$) but potentially a long $230.7^{+246.1}_{-218.1}$ kyr apparent burial duration indicating limited glacial erosion at this site (Sugden et al., 2005). Because the sum of apparent exposure and burial

Table 1
Test sample information from West Antarctica and northern Sweden

| Sample no. | Latitude (°) | Longitude (°) | Altitude (m a.s.l.) | $^{10}Be$ concentration ($10^5$ atom/g) | $^{10}Be$ production rate (atom/g/yr) | $^{26}Al$ concentration ($10^5$ atom/g) | $^{26}Al$ production rate (atom/g/yr) | $^{26}Al/^{10}Be$ ratio |
|---|---|---|---|---|---|---|---|---|
| *West Antarctica*[a] | | | | | | | | |
| 01-MBL-132-BBD | −77.074 | 145.699 | 791 | 14.33±0.24 | 13.1±0.8 | 79.12±1.96 | 79.9±4.8 | 5.52±0.17 |
| 01-MBL-131-BBD | −77.074 | 145.699 | 789 | 11.65±0.24 | 12.7±0.8 | 62.16±1.56 | 77.7±4.7 | 5.34±0.17 |
| 01-MBL-144-REA | −77.077 | 145.587 | 685 | 4.96±0.12 | 11.7±0.7 | 27.63±0.55 | 71.2±4.3 | 5.57±0.18 |
| 01-MBL-148-REA | −77.071 | 145.595 | 616 | 4.60±0.12 | 11.0±0.7 | 24.47±0.40 | 66.8±4.0 | 5.32±0.16 |
| 01-MBL-150-REA | −77.068 | 145.575 | 489 | 0.44±0.04 | 9.7±0.6 | 2.37±0.17 | 59.4±3.6 | 5.41±0.65 |
| *Northern Sweden*[b] | | | | | | | | |
| 98-20 | 67.153 | 18.862 | 920 | 3.85±0.03 | 11.9±0.7 | 17.31±0.84 | 72.5±4.4 | 4.49±0.22 |
| 99-01 | 67.677 | 23.073 | 360 | 5.37±0.05 | 7.1±0.4 | 29.66±1.76 | 43.5±2.6 | 5.53±0.33 |
| 99-04 | 67.681 | 23.195 | 300 | 4.18±0.05 | 6.7±0.4 | 21.69±1.72 | 41.0±2.5 | 5.18±0.42 |
| 99-05 | 67.707 | 23.279 | 350 | 3.53±0.05 | 7.1±0.4 | 20.48±0.74 | 43.5±2.6 | 5.81±0.22 |

[a] West Antarctic data are from Sugden et al. (2005).
[b] Northern Sweden data are from Stroeven et al. (2002b, 2006). Sample 98-20 originally published in Fabel et al. (2002). Sample 99-05 is new data. Its location is close to the site of sample 99-06 in Stroeven et al. (2002b, "K" in Fig. 1, p. 146) and occurs at the same elevation.

Table 2
Calculated results for test data from West Antarctica and northern Sweden

| Sample no. | Apparent $^{10}$Be exposure age (kyr) | Apparent $^{26}$Al exposure age (kyr) | Mean apparent burial age[a] (kyr) | Minimum apparent burial age (kyr) | Maximum apparent burial age (kyr) | Mean cutoff value (‰) | Minimum cutoff value (‰) | Maximum cutoff value (‰) | Ratio difference (%) | Mean first-cut time[b] (kyr) | Minimum first-cut time (kyr) | Maximum first-cut time (kyr) |
|---|---|---|---|---|---|---|---|---|---|---|---|---|
| *West Antarctica* | | | | | | | | | | | | |
| 01-MBL-132-BBD | 112.2±7.1 | 104.2±7.2 | 192.0 | 133.7 | 252.2 | 4.07 | 3.94 | 4.57 | <0.1 | 6.9 | 6.1 | 9.0 |
| 01-MBL-131-BBD | 93.3±6.0 | 83.3±5.7 | 255.8 | 195.5 | 318.0 | 3.90 | 3.84 | 4.01 | <0.3 | 5.8 | 5.5 | 6.5 |
| 01-MBL-144-REA | 42.9±2.8 | 39.6±2.6 | 174.7 | 113.6 | 237.9 | 3.84 | 3.76 | 3.97 | <0.2 | 5.5 | 5.1 | 6.2 |
| 01-MBL-148-REA | 42.4±2.8 | 37.3±2.4 | 263.0 | 206.0 | 321.7 | 3.75 | 3.71 | 3.83 | <0.2 | 5.0 | 4.9 | 5.5 |
| 01-MBL-150-REA | 4.5±0.5 | 4.0±0.4 | 230.7 | 12.6 | 476.8 | 3.33 | 3.16 | 3.41 | <0.3 | 2.9 | 2.0 | 3.3 |
| *Northern Sweden* | | | | | | | | | | | | |
| 98-20 | 32.7±2.0 | 24.2±1.9 | 589.0 | 497.1 | 685.6 | 3.17 | 3.11 | 3.21 | <0.3 | 3.1 | 2.6 | 3.9 |
| 99-01 | 76.6±4.7 | 70.5±6.2 | 188.6 | 77.2 | 306.8 | 3.72 | 3.57 | 4.48 | <0.1 | 9.0 | 7.9 | 12.5 |
| 99-04 | 63.2±3.9 | 54.3±5.6 | 314.2 | 164.4 | 476.8 | 3.55 | 3.43 | 3.78 | <0.1 | 7.8 | 6.7 | 9.3 |
| 99-05 | 50.1±3.1 | 48.2±3.5 | 93.6 | 22.2 | 167.8 | 3.90 | 3.59 | 5.07 | <0.8 | 9.9 | 8.1 | 15.2 |

| Sample no. | Mean total exposure duration (kyr) | Minimum total exposure duration (kyr) | Maximum total exposure duration (kyr) | Mean total burial duration (kyr) | Minimum total burial duration (kyr) | Maximum total burial duration (kyr) | Mean total history (kyr) | Minimum total history (kyr) | Maximum total history (kyr) |
|---|---|---|---|---|---|---|---|---|---|
| *West Antarctica* | | | | | | | | | |
| 01-MBL-132-BBD | 120.0 | 113.4 | 127.1 | 284.2 | 117.5 | 439.5 | 404.2 | 230.9 | 566.6 |
| 01-MBL-131-BBD | 104.3 | 97.8 | 111.8 | 395.8 | 296.6 | 732.7 | 500.1 | 394.4 | 844.5 |
| 01-MBL-144-REA | 46.0 | 43.1 | 49.2 | 346.8 | 81.9 | 520.1 | 392.8 | 124.9 | 569.3 |
| 01-MBL-148-REA | 47.4 | 44.3 | 50.7 | 521.9 | 352.9 | 803.7 | 569.2 | 397.2 | 854.5 |
| 01-MBL-150-REA | 5.4 | 4.3 | 6.5 | 1237.4 | 322.7 | 2541.8 | 1242.8 | 327.0 | 2600.0[c] |
| *Northern Sweden* | | | | | | | | | |
| 98-20 | 44.9 | 38.8 | 50.4 | 2093.0 | 1066.9 | 2714.2 | 2137.9 | 1108.4 | 2753.0[c] |
| 99-01 | 83.2 | 77.5 | 90.3 | 316.2 | 41.0 | 693.3 | 399.4 | 118.4 | 783.5 |
| 99-04 | 72.9 | 66.1 | 81.8 | 706.0 | 194.5 | 913.3 | 778.9 | 260.7 | 995.1 |
| 99-05 | 52.3 | 49.6 | 55.6 | 150.9 | 0.2 | 344.5 | 203.1 | 49.8 | 400.1 |

[a]Apparent burial age is inferred from $^{26}$Al/$^{10}$Be ratio relative to ratio expected for continuous exposure (production ratio of 6.1). Maximum and minimum apparent burial ages are inferred using uncertainty (the minimum and maximum values) of the measured $^{26}$Al/$^{10}$Be ratio.
[b]First-cut time is the age of the youngest intersection between the climate record and the cutoff line indicating the last deglaciation age.
[c]The maximum total history approaches the limit of the climate proxy record.

durations represents the minimum estimate of the exposure-burial history (total history; Table 2) of a sample, the total history of the samples in this area could be much longer (>300 kyr). We used a marine benthic foraminifera oxygen isotope record from the South Atlantic (Shackleton, 1984) as the climate proxy record for the analysis.

The four summit samples yielded best-fit solutions with <0.3% differences between simulated and measured $^{26}Al/^{10}Be$ ratios. The best-fit cutoff values for the four samples are all close to each other, with an average value of $3.89^{+0.21}_{-0.08}$‰, and show a trend of increasing values with altitude (Fig. 3A). Because higher cutoff values indicate a longer exposure duration for the surface, the pattern of higher cutoff values with altitude is consistent with the expected pattern resulting from the thickening and thinning of the ice sheet and consequent changes in the ice surface elevation and burial

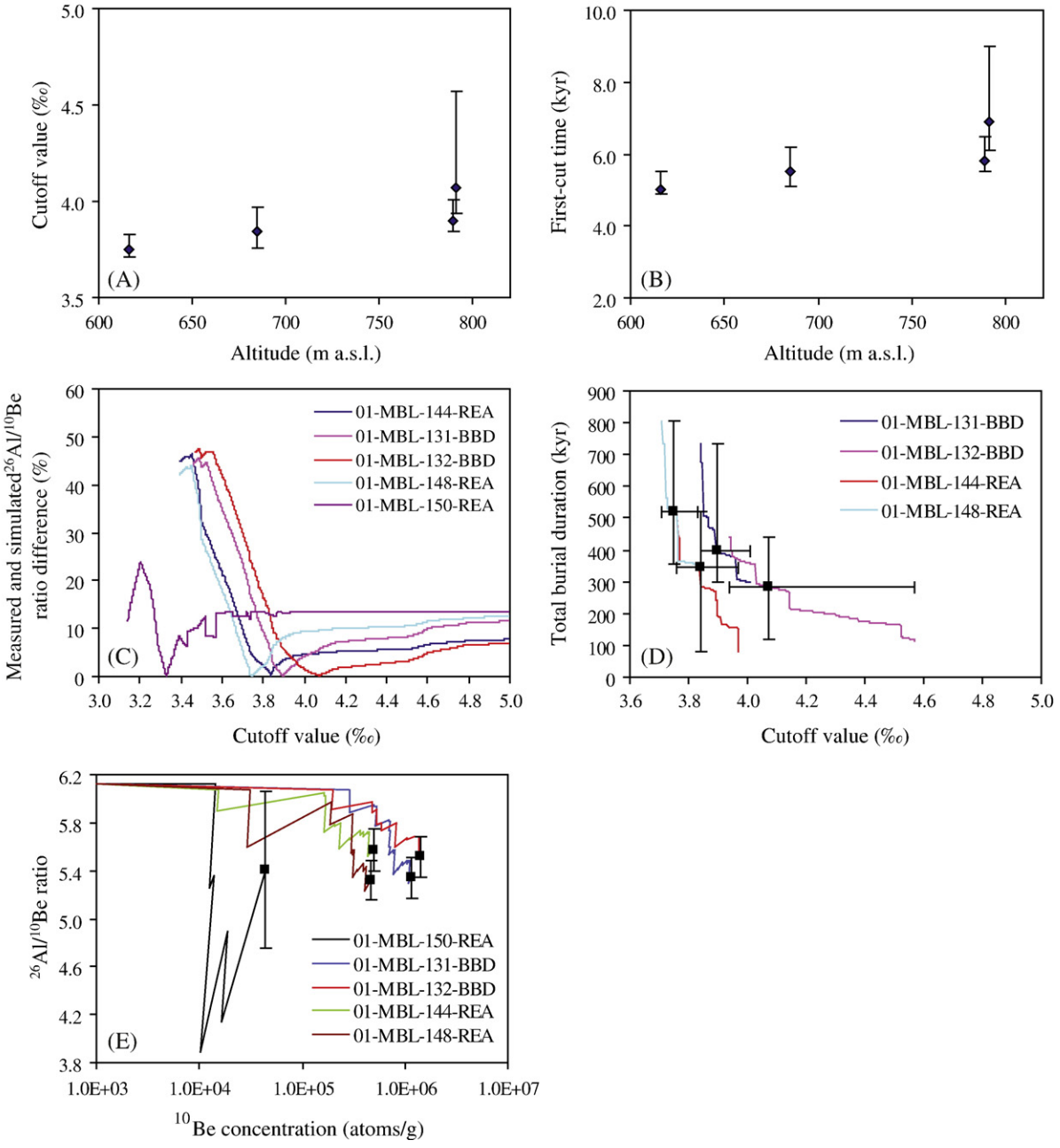


Fig. 3. Analytical results for West Antarctic samples. (A) and (B) Patterns of best-fit cutoff values and first-cut times (last deglaciation ages) with altitude. Cutoff values and deglaciation ages generally increase with elevation, consistent with progressive exposure of a topographic high as an ice sheet surface falls in elevation during deglaciation. (C) Differences between simulated and measured $^{26}Al/^{10}Be$ ratios for different cutoff values. (D) The relationship between the total burial duration and cutoff value. Step changes occur when a small change in a cutoff value results in a particular glaciation being included or excluded. (E) Variations of $^{26}Al/^{10}Be$ ratio with $^{10}Be$ concentration. Each curve plots the evolution of a sample's radionuclide concentrations over the course of successive exposure and burial periods. Sample 01-MBL-150-REA from the ice-moulded slope shows a distinctive different pattern from summit samples, reflecting the influence of erosion on radionuclide concentrations.

duration with altitude. In addition, because the age of the last (youngest) intersection between the climate record and the cutoff line (first-cut time) indicates the deglaciation age for the last glacial cycle at the sample location, its relationship with altitude reveals the pattern of deglaciation in the region, with earlier deglaciations at higher elevations (Fig. 3B). The sample from the ice-moulded slope also had a best-fit solution with <0.3% difference between simulated and measured $^{26}Al/^{10}Be$ ratios. Thus, even with a zero erosion assumption, samples from this erosion surface with inherited nuclide concentrations provided a best-fit that is internally consistent with measured $^{26}Al/^{10}Be$ ratios. However, the best-fit cutoff value of $3.33^{+0.08}_{-0.17}$‰ is significantly different from the other four samples, indicating different sample surface conditions (such as some subglacial erosion) or exposure-burial histories of this sample compared to the other samples.

Input uncertainties of $^{10}Be$ and $^{26}Al$ measurements (Table 2) result in a range of best-fit cutoff values. Plotting the differences between simulated and measured $^{26}Al/^{10}Be$ ratios against the corresponding cutoff values facilitates an assessment of the sensitivity of the results to cutoff values (Fig. 3C). If a certain level of uncertainty can be established as acceptable, for example 1% difference in simulated and measured $^{26}Al/^{10}Be$ ratio, then a range of cutoff values providing reasonable interpretations of the complex exposure-burial history for a sample can be obtained. From this we can identify samples that are highly sensitive (e.g., 01-MBL-144-REA) such that small changes in cutoff values will result in bigger changes in the difference of $^{26}Al/^{10}Be$ ratios than for other samples (e.g., 01-MBL-132-BBD).

For the range of cutoff values indicated by the analysis, a range of total exposure-burial histories can also be constrained. Derived information comprises the total exposure- and burial durations and total history (listed in Table 2), the number of glacial cycles, the exposure- and burial durations for each cycle, and the timing of onset and termination of glaciation at each site. The total exposure- and burial durations of a sample are also sensitive to the change of cutoff values. For example, plotting total burial duration against corresponding cutoff value clearly shows the sensitivity of this parameter to the change of cutoff values (Fig. 3D). Step changes in the total burial duration reflect changes in the numbers of glacial cycles associated with particular cutoff values.

Using the best-fit cutoff value, $^{10}Be$ and $^{26}Al$ concentrations for different exposure-burial periods interpreted from the climatic proxy record can be simulated and $^{26}Al/^{10}Be$ ratios calculated (Fig. 3E). With multiple samples, the pattern of $^{26}Al/^{10}Be$ ratio variations can be used to evaluate if the typical initial assumption of no erosion is appropriate. In this analysis, the sample from the ice-moulded slope (01-MBL-150-REA) shows a distinctively different pattern of ratio variations compared to the other four samples (Fig. 3E), indicating a different sample surface history compared to the summit samples. This is consistent with the interpretation that this sample was taken from a surface that experienced insufficient subglacial erosion (<2 m) to completely remove the preglacial nuclide inventory during exposure-burial cycles (Sugden et al., 2005).

### 3.2. Northern Sweden

The northern Swedish mountains and lowlands have been the seeding/core area for the Fennoscandian ice sheet during the Quaternary (Ljungner, 1949; Kleman, 1992; Mangerud et al., 1996; Kleman and Stroeven, 1997; Fredin, 2002). Many relict surfaces characterized by boulder fields and tors occur in this area, despite repeated episodes of burial by ice sheets. Such relict surfaces have been identified through mapping based on remote sensing, field investigation, and surface exposure dating (Kleman and Stroeven, 1997; Fabel et al., 2002; Hättestrand and Stroeven, 2002; Stroeven et al., 2002b; Goodfellow et al., in press). Four samples taken from relict surfaces with measured $^{10}Be$ and $^{26}Al$ concentrations are used here (Table 1). All samples indicate apparent exposure ages from 32.7±2.0 kyr to 76.6±4.7 kyr ($^{10}Be$) and apparent burial ages from $93.6^{+74.2}_{-71.4}$ to $589.0^{+96.6}_{-91.9}$ kyr inferred from $^{26}Al/^{10}Be$ ratios. The marine benthic foraminifera oxygen isotope record from DSDP 607 is used as the climate proxy record for this area. This record has previously been related to the pattern of ice advances and retreats in this area and has been used to reconstruct the ice occupation history for northern Sweden (Fabel et al., 2002; Stroeven et al., 2002b). Kleman and Stroeven (1997) proposed a cutoff value of $\delta^{18}O=3.7$‰ to define a temporal framework for ice-free and ice-covered conditions in this area, and so the analysis here provides a way to examine this cutoff value using an alternate approach.

The results for three sites in the northern Swedish lowlands (tors; samples 99-01, 99-04 and 99-05) yield similar but less consistent patterns as those obtained with the West Antarctic samples. They all yield fits with <0.8% difference between simulated best-fit and measured $^{26}Al/^{10}Be$ ratios. The relationships between cutoff values and altitude and between deglaciation ages and altitude show that higher altitude sites generally experienced longer exposure durations and thus earlier deglaciation ages than lower altitude sites (Fig. 4A,B). However, while this pattern is consistent for expectations of ice sheet behavior in the high-relief terrain in northern Sweden (Kleman and Stroeven, 1997) and consistent with available cosmogenic nuclide ages (Fabel et al., 2002; Stroeven et al., 2006), these samples come from a relatively low-elevation and low-relief setting (cf. Stroeven et al., 2002b). Hättestrand and Stroeven (2002) showed a pronounced spatial pattern of erosion and preservation in the area but discerned no elevational trends. Ice sheet retreat in this region between the Younger Dryas limit in northern Norway and final deglaciation in the northern Swedish mountains appears to have proceeded regularly (unpublished data, Stroeven et al., 2003) and commenced in this region around 11.0±3.0 ka (Stroeven et al., 2002b); a value indistinguishable from the deglaciation results derived using the new methodology (Fig. 4B).

The average cutoff value from samples 99-01, 99-04, and 99-05 is $3.72^{+0.72}_{-0.19}$‰, which is close to the $\delta^{18}O$ cutoff value of 3.7‰ used by Kleman and Stroeven (1997) to reconstruct the ice occupation history for mountain ice sheets in northern Sweden. This close correspondence in cutoff values, despite different approaches, lends support to the idea that this is an

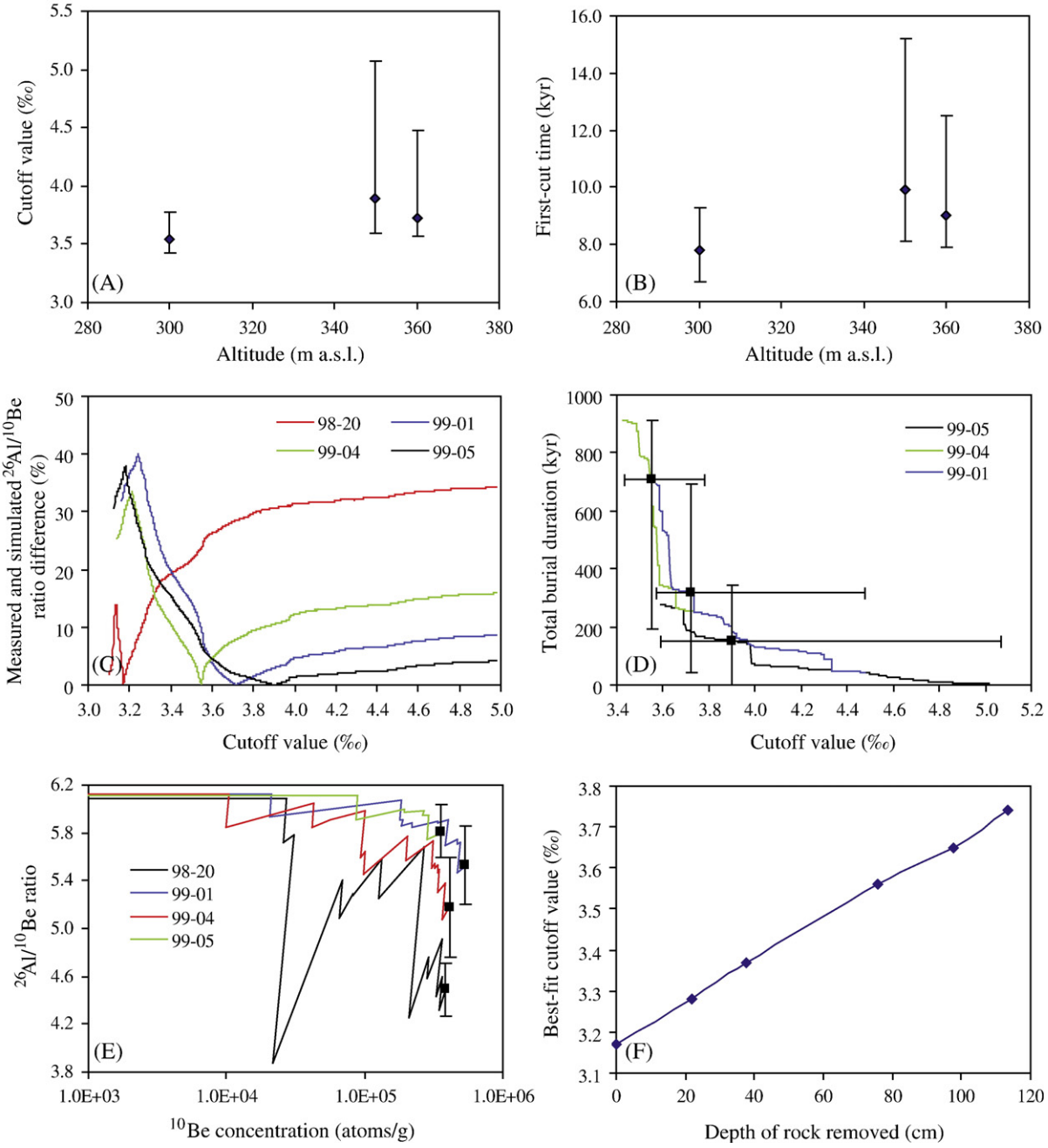


Fig. 4. Analytical results for samples from northern Sweden. (A) and (B) Patterns of best-fit cutoff values and first-cut times (last deglaciation ages) with altitude. (C) Differences between simulated and measured $^{26}Al/^{10}Be$ ratios for different cutoff values. (D) Relationship between the total burial duration and cutoff value. (E) Variations of $^{26}Al/^{10}Be$ ratio with $^{10}Be$ concentration. (F) Relationship between the best-fit cutoff value and depth of rock removed for sample 98-20 tested using a simple assumption that a certain depth of rock was suddenly removed during the last glacial cycle.

appropriate value for reconstructing ice occupation histories in this area using the DSDP 607 record.

Plotting the difference between simulated and measured $^{26}Al/^{10}Be$ ratios against the corresponding cutoff value can help to assess the sensitivity of the results to cutoff values (Fig. 4C). For these samples, sample 99-04 is more sensitive than the other two samples (99-01 and 99-05). Plotting total burial duration against corresponding cutoff values shows step changes in burial duration (indicating the numbers of glacial cycles) with changes in cutoff value (Fig. 4D).

Sample 98-20 was sampled from a relict bedrock surface at 920 m a.s.l. in the northern Swedish mountains (Fabel et al., 2002; Harbor et al., 2006). The best-fit solution for this sample has <0.3% difference between simulated and measured $^{26}Al/^{10}Be$ ratios. Due to its location near to the current water divide and its higher altitude, the best-fit cutoff value ($3.17^{+0.04}_{-0.06}$‰) and other parameters such as the first-cut time and total burial duration differ significantly from the three lowland tor samples. Also, the $^{26}Al/^{10}Be$ ratio variation shows a distinctively different pattern compared to the other three

samples (Fig. 4E). The most likely explanation for these differences is that they reflect different exposure-burial histories between the mountain and the lowland areas. Because the mountains were ice sheet seeding areas, glaciations typically started when advancing glaciers and ice caps merged into ice fields (Fredin, 2004), mountain ice sheets and eventually into Fennoscandian ice sheets (Kleman et al., 1997). It is therefore conceivable that sample 98-20 in the mountains experienced shorter exposure- and longer burial durations than the lowland tor samples as the latter typically were first covered when mountain ice sheets grew towards their maximum extent. The immediate implication is that the current mean total history (assuming zero surface erosion) derived in this study is more than 2000 kyr in contrast to the Fabel et al. (2002) estimate of 845 kyr using a 3.7‰ cutoff value.

Differences between the mountain and lowland sites may also be explainable if the assumption of zero surface erosion is not valid for sample 98-20. We tested this assumption using different combinations of subaerial- and glacial "steady state" erosion rates, but were unable to achieve the cutoff value of 3.7‰ used by Fabel et al. (2002) and derived for the lowland tor sites. This indicated that the difference is not the result of steady state erosion of the sample surface. We subsequently tested whether non-steady state erosion of the bedrock at sample site 98-20 could be invoked to explain the differences. This assumption was tested by simply assuming that a certain depth of rock was suddenly removed during the last glacial cycle. What was observed is that when the non-steady state erosion depth increases, the best-fit cutoff values increase as well (Fig. 4F). To reach a best-fit cutoff value of 3.7‰, about 110 cm of rock (or about 220 cm of regolith (assuming the density of regolith is about half of the bedrock density, 2.75 g $cm^{-3}$ used here in the calculation), or a combination of these) had to be removed. While this appears to be a plausible numerical solution, we are uncertain whether the sample site actually experienced so much erosion. The sample is located in a relict patch near a subglacial sliding boundary (Harbor et al., 2006). However, in the absence of a detailed understanding of the hydrology of subglacial sliding boundaries, the patchy removal of regolith and bedrock within a relict surface and close to a sliding boundary (by localized refreezing, perhaps) must be considered as potentially plausible.

## 4. Discussion and conclusions

Combining measured concentrations of multiple cosmogenic nuclides with a climate proxy record that is believed to reflect a temporal pattern of burial by ice and exposure for a given sample site provides a novel way to interpret the complex exposure-burial (total) history for bedrock surfaces that have been preserved despite a series of glaciations. By simulating nuclide concentrations based on the modeled temporal record of exposure and burial dictated by specific glacial/non-glacial cutoff values for the climate proxy record, and comparing the simulated nuclide concentrations to measured nuclide concentrations and ratios, a best-fit cutoff value for the climate proxy record can be determined. In addition, the sensitivity of the simulated nuclide concentrations to cutoff values can be assessed. This allows the total history of a surface to be interpreted and allows the user to evaluate how many glacial cycles a surface has survived and thus gain significant insights into ice sheet dynamics and landscape evolution under ice sheets.

Test data from West Antarctic nunataks and northern Swedish mountain and lowland sites indicate that the method is robust and that previous work for the Swedish lowland sites used a cutoff value that is essentially identical to the best-fit value determined by this method. Sensitivity analyses indicate that small changes in cutoff values can yield step changes in results. Thus, assessing the sensitivity of results to variations in cutoff values is critical when using this method. The analysis yields best-fit cutoff values that vary with altitude, which is consistent with realistic glaciological histories of ice sheet thinning and thickening across the sites. Because the method uses an analysis of $^{26}Al/^{10}Be$ ratio variations with changing exposure-burial durations it can be used to assess whether the assumption of zero erosion of sampled surfaces is appropriate, and to evaluate which climate proxy record is most appropriate for an area if multiple climate proxy records are available.

However, the application of this method has several limitations. First, measurement uncertainties for cosmogenic nuclides result in a range of possible cutoff values and exposure-burial histories, commensurate with the size of the measurement error. Second, the application of this method is limited by the applicability, resolution, precision, and time range of the applied climate proxy record. Third, an underlying assumption of this approach is that proxy records can be used to study the volumetric behavior of a specific ice sheet. While this rather crude approximation can be accepted more easily for ice sheet interior locations, such as those considered for northern Sweden (Fabel et al., 2002; Stroeven et al., 2002a,b), its adaptation to ice marginal locations involves considerably more uncertainty. For example, rather small changes in glacial conditions in the ice sheet interior (such as a thinning which does not affect full ice sheet coverage of the area) can result in dramatic changes in the location of ice sheet margins (such as a significant ice sheet retreat leaving areas formerly ice-covered now ice-free). Thus, exposure-burial histories can be more confidently inferred for interior locations and the build up and decay of cosmogenic nuclides with different half lives can be simulated for these locations, provided that the surfaces studied are all relict surfaces. The West Antarctic samples are also located away from the ice sheet margin as these were sampled from the summit and flanks of a nunatak. Here, it is the history of the "inland" ice sheet surface elevation (above and below the sample sites) that is monitored by the cosmogenic isotopes. This measure is more stable in relation to climate proxy values than are marginal locations.

With these limitations in mind the approach will be a valuable tool for Quaternary geologists, geomorphologists, glaciologists, and ice sheet modelers in reconstructing ice sheet histories and in providing constraints on the geomorphic impacts of multiple glaciations.

## Acknowledgements

This work was supported by the National Science Foundation Grant OPP-0138486 to Harbor and Swedish Research Council Grant G-AA/GU 621-2001-2331 to Stroeven. We thank Dr. Richard Marston for the detailed editing and suggestions for improvements and Dr. Mike Bentley and two anonymous reviewers for providing numerous constructive suggestions.

## References

Balco, G., Stone, J.O.H., Porter, S.C., Caffee, M.W., 2002. Cosmogenic-nuclide ages for New England coastal moraines, Martha's Vineyard and Cape Cod, Massachusetts, USA. Quaternary Science Reviews 21, 2127–2135.

Bierman, P.R., Marsella, K.A., Patterson, C., Davis, P.T., Caffee, M., 1999. Mid-Pleistocene cosmogenic minimum-age limits for pre-Wisconsinan glacial surfaces in southwestern Minnesota and southern Baffin Island: a multiple nuclide approach. Geomorphology 27, 25–39.

Bintanja, R., van de Wal, R.S.W., Oerlemans, J., 2002. Global ice volume variations through the last glacial cycle simulated by a 3-D ice-dynamical model. Quaternary International 95–96, 11–23.

Bintanja, R., van de Wal, R.S.W., Oerlemans, J., 2005. Modelled atmospheric temperatures and global sea levels over the past million years. Nature 437, 125–128.

Briner, J.P., Swanson, T.W., 1998. Using inherited cosmogenic $^{36}$Cl to constrain glacial erosion rates of the Cordilleran ice sheet. Geology 26, 3–6.

Briner, J.P., Miller, G.H., Davis, P.T., Bierman, P.R., Caffee, M., 2003. Last Glacial Maximum ice sheet dynamics in Arctic Canada inferred from young erratics perched on ancient tors. Quaternary Science Reviews 22, 437–444.

Brook, E.J., Kurz, M.D., Ackert Jr., R.P., Denton, G.H., Brown, E.T., Raisbeck, G.M., Yiou, F., 1993. Chronology of Taylor Glacier advances in Arena Valley, Antarctica, using *in situ* cosmogenic $^{3}$He and $^{10}$Be. Quaternary Research 39, 11–23.

Brook, E.J., Nesje, A., Lehman, S.J., Raisbeck, G.M., Yiou, F., 1996. Cosmogenic nuclide exposure ages along a vertical transect in western Norway: implications for the height of the Fennoscandian ice sheet. Geology 24, 207–210.

Davis, P.T., Bierman, P.R., Marsella, K.A., Caffee, M.W., Southon, J.R., 1999. Cosmogenic analysis of glacial terrains in eastern Canadian Arctic: a test for inherited nuclides and the effectiveness of glacial erosion. Annals of Glaciology 28, 181–188.

Fabel, D., Harbor, J., 1999. The use of in-situ produced cosmogenic radionuclides in glaciology and glacial geomorphology. Annals of Glaciology 28, 103–110.

Fabel, D., Harbor, J., Dahms, D., James, A., Elmore, D., Horn, L., Daley, K., Steele, C., 2004. Spatial patterns of glacial erosion at a valley scale derived from terrestrial cosmogenic Be-10 and Al-26 concentrations in rock. Annals of the Association of American Geographers 94, 241–255.

Fabel, D., Stroeven, A.P., Harbor, J., Kleman, J., Elmore, D., Fink, D., 2002. Landscape preservation under Fennoscandian ice sheets determined from in situ produced $^{10}$Be and $^{26}$Al. Earth and Planetary Science Letters 201, 397–406.

Fredin, O., 2002. Glacial inception and Quaternary mountain glaciations in Fennoscandia. Quaternary International 95–96, 99–112.

Fredin, O., 2004. Mountain Centered Icefields in Northern Fennoscandia, Dissertation No. 29, Department of Physical Geography and Quaternary Geology, Stockholm University, Sweden, 17 pp.

Goodfellow, B.W., 2007. Relict non-glacial surfaces in formerly glaciated landscapes. Earth-Science Reviews 80, 47–73.

Goodfellow, B.W., Stroeven, A.P., Hättestrand, C., Kleman, J., Jansson, K.N., in press. Deciphering a non-glacial/glacial landscape mosaic in the northern Swedish mountains. Geomorphology. doi: 10.1016/j.geomorph.2007.02.018.

Gosse, J.C., Phillips, F.M., 2001. Terrestrial in situ cosmogenic nuclides: theory and application. Quaternary Science Reviews 20, 1475–1560.

Harbor, J., Stroeven, A.P., Fabel, D., Clarhäll, A., Kleman, J., Li, Y.K., Elmore, D., Fink, D., 2006. Cosmogenic nuclide evidence for minimal erosion across two subglacial sliding boundaries of the late glacial Fennoscandian ice sheet. Geomorphology 75, 90–99.

Hättestrand, C., Stroeven, A.P., 2002. A relict landscape in the centre of Fennoscandian glaciation: Geomorphological evidence of minimal Quaternary glacial erosion. Geomorphology 44, 127–143.

Kleman, J., 1992. The palimpsest glacial landscape in northwestern Sweden — Late Weichselian deglaciation landforms and traces of older west-centered ice sheets. Geografiska Annaler 74A, 305–325.

Kleman, J., Stroeven, A.P., 1997. Preglacial surface remnants and Quaternary glacial regimes in northwestern Sweden. Geomorphology 19, 35–54.

Kleman, J., Hättestrand, C., Borgström, I., Stroeven, A., 1997. Fennoscandian paleoglaciology reconstructed using a glacial geological inversion model. Journal of Glaciology 43, 283–299.

Lal, D., 1991. Cosmic ray labeling of erosion surfaces: in situ nuclide production rates and erosion models. Earth and Planetary Science Letters 104, 424–439.

Landvik, J.Y., Brook, E.J., Gualtieri, L., Raisbeck, G., Salvigsen, O., Yiou, F., 2003. Northwest Svalbard during the last glaciation: ice-free areas existed. Geology 31, 905–908.

Lazarus, D., Spencer-Cervato, C., Pika-Biolzi, M., Beckmann, J.P., vonSalis, K., Hilbrecht, H., Thierstein, H., 1995. Revised Chronology of Neogene DSDP Holes from the World Ocean, Ocean Drilling Program. Technical Report, vol. 24. College of Geosciences, Texas A&M University, College Station, TX. 301 pp.

Li, Y.K., Harbor, J., Stroeven, A.P., Fabel, D., Kleman, J., Fink, D., Caffee, M., Elmore, D., 2005. Ice sheet erosion patterns in valley systems in northern Sweden investigated using cosmogenic nuclides. Earth Surface Processes and Landforms 30, 1039–1049.

Ljungner, E., 1949. East–west balance of the Quaternary ice caps in Patagonia and Scandinavia. Bulletin of the Geological Institutions of the University of Uppsala 33, 11–96.

Mangerud, J., Jansen, E., Landvik, J.Y., 1996. Late Cenozoic history of the Scandinavian and Barents Sea ice sheets. Global and Planetary Change 12, 11–26.

Marquette, G.C., Gray, J.T., Gosse, J.C., Courchesne, F., Stockli, L., Macpherson, G., Finkel, R., 2004. Felsenmeer persistence under non-erosive ice in the Torngat and Kaumajet mountains, Quebec and Labrador, as determined by soil weathering and cosmogenic nuclide exposure dating. Canadian Journal of Earth Sciences 41, 19–38.

Marsella, K.A., Bierman, P.R., Davis, P.T., Caffee, M.W., 2000. Cosmogenic $^{10}$Be and $^{26}$Al ages for the Last Glacial Maximum, eastern Baffin Island, Arctic Canada. Geological Society of America Bulletin 112, 1296–1312.

Napieralski, J., Hubbard, A., Li, Y.K., Harbor, J., Stroeven, A.P., Kleman, J., Alm, G., Jansson, K.N., 2007. Towards a GIS assessment of numerical ice-sheet model performance using geomorphological data. Journal of Glaciology 53, 71–83.

Nesje, A., Dahl, S.O., Linge, H., Ballantyne, C.K., McCarroll, D., Brook, E.J., Raisbeck, G.M., Yiou, F., 2007. The surface geometry of the Last Glacial Maximum ice sheet in the Andøya–Skånland region, northern Norway, constrained by surface exposure dating and clay mineralogy. Boreas 36, 227–239.

Phillips, W.M., Hall, A.M., Mottram, R., Fifield, L.K., Sugden, D.E., 2006. Cosmogenic $^{10}$Be and $^{26}$Al exposure ages of tors and erratics, Cairngorm Mountains, Scotland: timescales for the development of a classic landscape of selective linear glacial erosion. Geomorphology 73, 222–245.

Rinterknecht, V.R., Clark, P.U., Raisbeck, G.M., Yiou, F., Bitinas, A., Brook, E.J., Marks, L., Zelcs, V., Lunkka, J.P., Pavlovskaya, I.E., Piotrowski, J.A., Raukas, A., 2006. The last deglaciation of the southeastern sector of the Scandinavian Ice Sheet. Science 311, 1449–1452.

Rinterknecht, V.R., Clark, P.U., Raisbeck, G.M., Yiou, F., Brook, E.J., Tschudi, S., Lunkka, J.P., 2004. Cosmogenic $^{10}$Be dating of the Salpausselkä I Moraine in southwestern Finland. Quaternary Science Reviews 23, 2283–2289.

Rinterknecht, V.R., Marks, L., Piotrowski, J.A., Raisbeck, G.M., Yiou, F., Brook, E.J., Clark, P.U., 2005. Cosmogenic $^{10}$Be ages on the Pomeranian Moraine, Poland. Boreas 34, 186–191.

Rinterknecht, V.R., Pavlovskaya, I.E., Clark, P.U., Raisbeck, G.M., Yiou, F., Brook, E.J., 2007. Timing of the last deglaciation in Belarus. Boreas 36, 307–313.

Shackleton, N.J., 1984. Oxygen isotope evidence for Cenozoic climate change. In: Brenchley, P. (Ed.), Fossils and Climate. Wiley and Sons, New York, pp. 27–34.

Shackleton, N.J., Opdyke, N.D., 1973. Oxygen isotope and paleomagnetic stratigraphy of Equatorial Pacific core V28–238: oxygen isotope temperatures and ice volumes on a 10(5) and 10(6) year scale. Quaternary Research 3, 39–55.

Spielhagen, R.F., Baumann, K.H., Erlenkeuser, H., Nowaczyk, N.R., Norgaard-Pedersen, N., Vogt, C., Weiel, D., 2004. Arctic Ocean deep-sea record of northern Eurasian ice sheet history. Quaternary Science Reviews 23, 1455–1483.

Staiger, J.K.W., Gosse, J.C., Johnson, J.V., Fastook, J., Gray, J.T., Stockli, D.F., Stockli, L., Finkel, R., 2005. Quaternary relief generation by polythermal glacier ice. Earth Surface Processes and Landforms 30, 1145–1159.

Steig, E.J., Wolfe, A.P., Miller, G.H., 1998. Wisconsinan refugia and the glacial history of eastern Baffin Island, Arctic Canada: coupled evidence from cosmogenic isotopes and lake sediments. Geology 26, 835–838.

Stone, J.O., Balco, G.A., Sugden, D.E., Caffee, M.W., Sass III, L.C., Cowdery, S.G., Siddoway, C., 2003. Holocene deglaciation of Marie Byrd Land, West Antarctica. Science 299, 99–102.

Stone, J.O., Ballantyne, C.K., Fifield, L.K., 1998. Exposure dating and validation of periglacial weathering limits, northwest Scotland. Geology 26, 587–590.

Stroeven, A.P., Fabel, D., Dahlgren, K.I.T., Harbor, J., Hättestrand, C., Kleman, J., 2003. Tracing the post-Younger Dryas retreat of the northern Fennoscandian Ice Sheet using cosmogenic radionuclide exposure ages. Geological Society of America Abstracts With Programs 35, 388–389.

Stroeven, A.P., Fabel, D., Harbor, J., Hättestrand, C., Kleman, J., 2002a. Quantifying the erosional impact of the Fennoscandian ice sheet in the Torneträsk–Narvik corridor, northern Sweden, based on cosmogenic radionuclide data. Geografiska Annaler 84A, 275–287.

Stroeven, A.P., Fabel, D., Hättestrand, C., Harbor, J., 2002b. A relict landscape in the centre of Fennoscandian glaciation: cosmogenic radionuclide evidence of tors preserved through multiple glacial cycles. Geomorphology 44, 145–154.

Stroeven, A.P., Harbor, J., Fabel, D., Kleman, J., Hättestrand, C., Elmore, D., Fink, D., Fredin, O., 2006. Slow, patchy landscape evolution in northern Sweden despite repeated ice-sheet glaciation. Special Paper, vol. 398. Geological Society of America, Boulder, CO, pp. 387–396.

Sugden, D.E., Balco, G., Cowdery, S.G., Stone, J.O., Sass III, L.C., 2005. Selective glacial erosion and weathering zones in the coastal mountains of Marie Byrd Land, Antarctica. Geomorphology 67, 317–334.

Tschudi, S., Ivy-Ochs, S., Schlüchter, C., Kubik, P., Rainio, H., 2000. $^{10}$Be dating of Younger Dryas Salpausselkä I formation in Finland. Boreas 29, 287–293.

Turco, E., Hilgen, F.J., Lourens, L.J., Shackleton, N.J., Zachariasse, W.J., 2001. Punctuated evolution of global climate cooling during the late Middle to early Late Miocene: high-resolution planktonic foraminiferal and oxygen isotope records from the Mediterranean. Paleoceanography 16, 405–423.

van den Berg, J., 2007. Interactions Between Ice Sheets, Climate and the Solid Earth. Doctoral dissertation, Utrecht University, 146 p.

Vidal, L., Bickert, T., Wefer, G., Rohl, U., 2002. Late Miocene stable isotope stratigraphy of SE Atlantic ODP Site 1085: relation to Messinian events. Marine Geology 180, 71–85.

Westerhold, T., Bickert, T., Rohl, U., 2005. Middle to late Miocene oxygen isotope stratigraphy of ODP site 1085 (SE Atlantic): new constrains on Miocene climate variability and sea-level fluctuations. Palaeogeography, Palaeoclimatology, Palaeoecology 217, 205–222.